Biogeosciences
Discussions

Open Access

EGU

1 # **Particulate barium tracing significant mesopelagic carbon**

2 # **remineralisation in the North Atlantic**

3 **Nolwenn Lemaitre [1,2], Hélène Planquette[1], Frédéric Planchon[1], Géraldine Sarthou[1],**

4 **Stéphanie Jacquet[3], Maribel I. García-Ibáñez[4], Arthur Gourain[1,5], Marie Cheize[1], Laurence**

5 **Monin[6], Luc André[6], Priya Laha[7], Herman Terryn[7] and Frank Dehairs[2]**

6

7 [1]Laboratoire des Sciences de l'Environnement Marin (LEMAR), UMR 6539, IUEM, Technopôle Brest Iroise, 29280
8 Plouzané, France

9 [2]Vrije Universiteit Brussel, Analytical, Environmental and Geo-Chemistry, Earth System Sciences research group,
10 Brussels, Belgium

11 [3]Aix Marseille Université, CNRS/INSU, Université de Toulon, IRD, Mediterranean Institute of Oceanography (MIO),
12 UM 110, 13288 Marseille, France

13 [4]Instituto de Investigaciones Marinas, IIM-CSIC, Eduardo Cabello 6, 36208 Vigo, Spain

14 [5]Ocean Sciences Department, School of Environmental Sciences, University of Liverpool, Liverpool L69 3GP, United
15 Kingdom

16 [6]Earth Sciences Department, Royal Museum for Central Africa, Leuvensesteenweg 13, Tervuren, 3080, Belgium

17 [7]Vrije Universiteit Brussel, SURF research group, department of Materials and Chemistry, Brussels, Belgium

18 *Correspondance to:* Nolwenn Lemaitre, Department of Earth Sciences, Institute of Geochemistry and Petrology, ETH-
19   Zürich, Zürich, Switzerland. (nolwenn.lemaitre@erdw.ethz.ch)

20 **Keywords:** Particulate biogenic barium; Carbon remineralisation; North Atlantic; Biological pump

21 **Abstract**
22 The remineralisation of sinking particles by prokaryotic heterotrophic activities is important for controlling oceanic
23 carbon sequestration. Here, we report mesopelagic particulate organic carbon (POC) remineralisation fluxes in the
24 North Atlantic along the GEOTRACES-GA01 section (GEOVIDE cruise; May-June 2014) using the particulate
25 biogenic barium (excess barium; Ba_{xs}) proxy. Important mesopelagic (100–1000 m) Ba_{xs} differences were observed
26 along the transect depending on the intensity of past blooms, the phytoplankton community structure and the physical
27 forcing, including downwelling. The subpolar province was characterized by the highest mesopelagic Ba_{xs} content (up
28 to 727 pmol L^{-1}), which was attributed to an intense bloom averaging 6 mg Chl-*a* m^{-3} between January and June 2014
29 and by an intense 1500 m-deep convection in the central Labrador Sea during the winter preceding the sampling. This
30 downwelling could have promoted a deepening of the prokaryotic heterotrophic activity, increasing the Ba_{xs} content.
31 In comparison, the temperate province, characterized by the lowest Ba_{xs} content (391 pmol L^{-1}), was sampled during

Biogeosciences
Discussions

32 the bloom period and phytoplankton appear to be dominated by small and calcifying species, such as coccolithophorids.

33 The Ba_{xs} content, related to an oxygen consumption, was converted into a remineralisation flux using an updated

34 relationship, proposed for the first time in the North Atlantic. The estimated fluxes were in the same order of magnitude

35 than other fluxes obtained by independent methods (moored sediment traps, incubations) in the North Atlantic.

36 Interestingly, in the subpolar and subtropical provinces, mesopelagic POC remineralisation fluxes (up to 13 and 4.6

37 mmol C m^{-2} d^{-1}, respectively) were equalling and occasionally even exceeding upper ocean POC export fluxes,

38 highlighting the important impact of the mesopelagic remineralisation on the biological carbon pump with a near-zero,

39 deep (> 1000 m) carbon sequestration efficiency in spring 2014.

40 **1. Introduction**

41 The oceanic biological carbon pump (BCP) controls the export of carbon and nutrients to the deep ocean, especially

42 through the production of biogenic sinking particles. In the North Atlantic, the oceanic BCP is particularly efficient in

43 transporting carbon to the deep ocean (Buesseler et al., 1992; Buesseler and Boyd, 2009; Herndl and Reinthaler, 2013;

44 Honjo and Manganini, 1993; Le Moigne et al., 2013b) due to its strong spring bloom (Henson et al., 2009; Pommier

45 et al., 2009), and it is estimated to contribute up to 18% of the BCP in the world's ocean (Sanders et al., 2014).

46 However, the efficiency of this transfer depends on many processes including the remineralisation intensity occurring

47 within the mesopelagic layer (100–1000 m depth layer). In the mesopelagic layer, most of the particulate organic

48 carbon (POC) exported from surface is released to the dissolved phase, i.e., dissolved organic carbon (DOC; Buesseler

49 et al., 2007; Buesseler and Boyd, 2009; Burd et al., 2016; Herndl and Reinthaler, 2013; Lampitt and Antia, 1997;

50 Martin et al., 1987). Mesopelagic remineralisation has been often reported to exceed the carbon supplies (i.e. POC and

51 DOC; Aristegui et al., 2009; Baltar et al., 2009; Burd et al., 2010; Collins et al., 2015; Fernández-castro et al., 2016;

52 Giering et al., 2014; Reinthaler et al., 2006), highlighting the importance of the mesopelagic layer on the fate of the

53 sinking POC, and occasionally questioning the efficiency of the North Atlantic to transfer POC to the deep ocean.

54 In this context, we examined mesopelagic POC remineralisation along the GEOTRACES-GA01 section during the

55 GEOVIDE cruise (15 May–30 June, 2014; R/V Pourquoi Pas?) by assessing particulate biogenic barium (excess

56 barium; Ba_{xs}) contents. The accumulation of Ba_{xs} in the mesopelagic layer has been related to the presence of barite

57 ($BaSO_4$) crystals, which appear to be formed by biological activity in the upper water column (Bishop, 1988; Cao et

58 al., 2016; Dehairs et al., 1980; Horner et al., 2015). The micro-sized barite crystals precipitate inside oversaturated

59 micro-environments, mostly aggregates of organic material where prokaryotic activity is intense (Bishop, 1988; Collier

60 and Edmond, 1984; Dehairs et al., 1980; Ganeshram et al., 2003; Gonzalez-Munoz et al., 2003). When these aggregates

61 are remineralised, barite crystals are released within the mesopelagic layer. Therefore, the Ba_{xs} content can be related

62 to an oxygen consumption (Dehairs et al., 1997; Shopova et al., 1995) and then converted to a remineralised POC flux

63 in the mesopelagic layer (Dehairs et al., 1997). Ba_{xs} has been successfully used as a proxy of remineralised POC flux

64 in the Southern (Cardinal et al., 2005; Jacquet et al., 2008a, 2008b, 2011, 2015; Planchon et al., 2013) and Pacific

65 Oceans (Dehairs et al., 2008).

66 This study is the first one to report the use of the Ba_{xs} proxy in the North Atlantic. Regional variations of the Ba_{xs}

67 distributions along the biogeochemical provinces are discussed regarding the stage and intensity of the bloom, the

68 phytoplankton community structure and the physical forcing. We re-assessed the algorithm between Ba_{xs} content and

69 oxygen consumption developed for the Southern Ocean, adapting it for the North Atlantic. We compared the

70 remineralisation fluxes resulting from this new North Atlantic-specific algorithm with those obtained by other methods

71 in the same area. This comparison, in combination with surface primary production (PP) and POC export estimates

72 (Lemaitre et al., in prep.), allowed us to investigate the fate of POC to the deep ocean in order to better constrain the

73 BCP and its efficiency in the North Atlantic.

74 **2. Methods**

75 **2.1. Study area**

76 The GEOVIDE section (15 May–30 June 2014; R/V Pourquoi pas?) crossed different biogeochemical provinces in the

77 North Atlantic including the North Atlantic subtropical gyre (NAST; Stations 1 and 13), the North Atlantic drift

78 (NADR) covering the West European (Stations 21 and 26) and Icelandic (Stations 32 and 38) basins, and the Atlantic

79 Arctic (ARCT) divided between the Irminger (Stations 44 and 51) and Labrador (Stations 64, 69 and 77) Seas

80 (Longhurst, 1995; Fig. 1, 2).

81 The evolution of chlorophyll-*a* (Chl-*a*) concentrations from satellite imagery (Fig. 1) revealed the decline of the bloom

82 in the NAST and the Labrador Sea and the bloom period within the NADR province and the Irminger Sea (Lemaitre et

83 al., in prep.). Indeed, the highest daily PP rates were measured in the NADR and in the Irminger Sea (> 150 mmol

84 C m^{-2} d^{-1}; A. Roukaerts, D. Fonseca Batista and F. Deman, unpublished data). The phytoplankton community structure

85 also varied regionally, with diatoms dominating the ARCT province and the West European basin of the NADR,

86 coccolithophorids dominating the Icelandic basin of the NADR and cyanobacteria in the NAST province (Tonnard et

87 al., 2017, this issue). Finally, as specifically described elsewhere (Daniault et al., 2016; García-Ibáñez et al., 2015;

88 Kieke and Yashayaev, 2015; Zunino et al., 2017; this issue), these provinces also differ in terms of their hydrographic

89 features, in particular, the presence of the sub-arctic front (SAF; which during GEOVIDE was located near Station

90 26), strong currents near the Greenland margin (probably influencing Stations 51 and 64), and an intense 1500 m-deep

91 convection in the central Labrador Sea (Station 69) due to the formation of the Labrador Sea Water (LSW) in winter.

92 These features influenced the magnitude of the carbon export fluxes, as well as the export and transfer efficiencies

93 along the transect (Lemaitre et al., in prep.). The highest POC export fluxes from the upper-ocean was observed in the

94 NADR province and in the Labrador Sea, reaching 8.4 ± 0.5 and 10 ± 0.8 mmol C m^{-2} d^{-1} at Stations 32 and 69,

95 respectively. Export efficiency (e.g. POC export flux divided by PP) was generally low (≤ 12%), except at Stations 1

96 and 69 where it reached 30%. The transfer efficiency (e.g. upper ocean POC export flux divided by POC export flux

97 at 400 m) was more variable, ranging from 2% at Station 21 to 78% at Station 64 (Lemaitre et al., in prep.).

98 **2.2. Sampling and analyses**

99 In this study, we present two datasets of Ba$_{xs}$ concentrations:

100 1) Ba$_{xs}$ concentrations measured in samples collected using a standard CTD rosette equipped with 12 L Niskin

101 bottles. Generally, 18 depths were sampled between surface and 1500 m in order to obtain a high depth resolution of

102 the Ba$_{xs}$ signal at stations where primary production and POC export fluxes were also determined (Table S1).

103 Four to eight litters of seawater were filtered on acid-cleaned polycarbonate membranes of 0.4 µm porosity

104 (Nuclepore®, 47 or 90 mm diameter). Filter membranes were rinsed with Milli-Q water (18.2 MΩ cm; ≤ 5 mL) to

105   remove sea-salt, dried at ambient temperature under a laminar flow hood and finally stored in clean petri slides until

106   analysis.

107   In the laboratory, filters were totally digested with a concentrated tri-acid mixture (1.5 mL HCl / 1 mL HNO_3 / 0.5 mL

108   HF; all Merck suprapur grades) in clean Teflon vials (Savillex®) on a hot plate at 90°C, overnight. Then, the acid

109   solution was evaporated at 110°C until near dryness, and the residue was dissolved in 13 mL 0.32M HNO_3 (Merck;

110   distilled Normapur). The solutions, in polypropylene tubes (VWR), were analysed for Barium (Ba), Aluminium (Al)

111   and other major and minor elements using an inductively coupled plasma-quadrupole mass spectrometer (ICP-QMS;

112   X Series 2 Thermo Fisher) equipped with a collision cell technology (CCT). We used a concentric quartz nebulizer (1

113   mL min^{-1}) and nickel sample and skimmer cones. During the analyses, internal standards (Ru, In, Re and Bi) were

114   added to samples in order to monitor and correct the instrumental drift and matrix-dependent sensitivity variations.

115   Two multi-element artificial standard solutions were prepared for external calibration. The first contained major

116   elements (Na, Mg, Al, Ca and Ti) and the second was prepared with minor elements (Sr, Ba, REEs, Th and U).

117   Standards were prepared by dilution of the multi-element mixed standard stock solutions to span the expected range

118   of sample concentrations, with concentrations in the standard curve spaced to cover potential sample variations.

119   The accuracy and precision of our analyses were assessed using the following Certified Reference Materials (CRM):

120   BHVO-1, JB-3, JGb-1 and SLRS-5 (Table 1).

121   The detailed procedure for sample preparation and analysis is given in Cardinal et al. (2001).

122   2) Ba_{xs} concentrations measured in samples collected using the trace metal clean rosette, equipped with

123   twenty-two 12 L Go-Flo bottles at higher spatial resolution but with a lower vertical resolution in the mesopelagic

124   layer. Indeed, the entire water column was sampled at 31 stations along the GEOVIDE transect. Details regarding

125   filtration, sample processing and analyses can be found in Gourain et al. (2017; this issue). Briefly, at each depth, two

126   size fractions were investigated: 0.45–5 µm using polysulfone filters (Supor®) and > 5 µm using mixed ester cellulose

127   filters (MF, Millipore®). Between 2 and 5 L of seawater were filtered for the upper water column (surface to 100 m)

128   and 10 L below 100 m. In the laboratory, filters were digested with a solution of 8 M HNO_3 (Ultrapur grade, Merck)

129   and 2.3 M HF (Suprapur grade, Merck). Vials were then refluxed at 130 °C on a hotplate during 4 h. After a gentle

130   evaporation, the residue was brought back into solution with approximately 2 mL of 0.32 M HNO_3 spiked with 1 µg

131   L^{-1} of Indium. Solutions were analysed using a SF-ICP-MS (Element 2, Thermo) following the method of Planquette

132   and Sherrell (2012). Total Ba and Al concentrations were calculated by adding the two size fractions. The accuracy

133   and precision of these analyses were assessed using the BCR-414 CRM (see Gourain et al., 2017; this issue).

134   For both datasets, the Ba_{xs} concentrations were calculated by subtracting the particulate lithogenic barium (pBa-litho)

135   from the total particulate barium (pBa). The pBa-litho was determined by multiplying the particulate aluminium (pAl)

136   concentration by the upper continental crust (UCC) molar Ba:Al ratio (0.00135 mol mol^{-1}; Taylor and Mclennan,

137   1985). Along the GEOVIDE section, pBa-litho represented less than 7 % of the total barium, except at Stations 1 and

138   53, close to the Iberian and Greenland margin, respectively, where pBa-litho accounted for 28 and 44 %, respectively.

139   Because of the rather large uncertainty associated with the UCC Ba:Al ratio and because of the strong lithogenic

140   particle loads there, Stations 1 and 53 were not considered further in this study. Uncertainties on Ba_{xs} were estimated

141   using error propagation and represented from 6 to 25 % of the Ba_{xs} concentrations.

142 At stations where total pBa and pAl concentrations were available at a similar depth, the comparison between the Ba_{xs}

143 concentrations obtained by the two sampling and analytical methods was excellent (regression slope: 0.94; r²: 71 %;

144 p<0.01; n=91; Fig. S1).

145 In addition, analyses of filtered suspended matter were carried out using a Field Emission Scanning Electron

146 Microscope (FE-SEM; JEOL JSM-7100F) to verify the relationship between Ba_{xs} and barite particles (Section 4.3.1).

147 For seven samples, we analysed a filter surface of 0.5 cm²: 6 samples with high mesopelagic Ba_{xs} concentrations

148 (Station 13 at 400 m; Station 38 at 300 m; Station 44 at 300 and 700 m; Station 69 at 600 m and Station 77 at 300 m)

149 and one sample with high surface Ba_{xs} concentrations (Station 26, 50 m).

150 **2.3. Determination of Carbon remineralisation fluxes**

151 In previous studies focusing on the Southern Ocean, Ba_{xs} based-mesopelagic carbon remineralisation fluxes were

152 estimated using Eq. (1), which relates the accumulated mesopelagic Ba_{xs} inventory to the rate of oxygen consumption

153 (Shopova et al., 1995; Dehairs et al., 1997):

154 $$JO_2 = (\text{mesopelagic } Ba_{xs} - Ba_{\text{ residual}}) / 17200 \qquad (1)$$

155 where *JO_2* is the rate of oxygen consumption (in µmol L^{-1} d^{-1}), *mesopelagic Ba_{xs}* is the depth-weighted average in the

156 mesopelagic layer (DWA; in pmol L^{-1}), *$Ba_{residual}$* is the deep-ocean Ba_{xs} value observed at zero oxygen consumption

157 (or Ba_{xs} background signal), which was determined to reach 180 pmol L^{-1} (Dehairs et al., 1997). Then, the oxygen

158 consumption JO_2 can be converted into C remineralised trough Eq. (2):

159 $$POC \text{ mesopelagic remineralisation} = Z \times JO_2 \times (C:O_2)_{\text{Redfield Ratio}} \qquad (2)$$

160 where the POC mesopelagic remineralisation is in mmol C m^{-2} d^{-1}, *Z* is the thickness of the layer in which the

161 mesopelagic Ba_{xs} is calculated, *JO_2* is the rate of oxygen consumption given by Eq. (1) and *$(C:O_2)_{Redfield\ Ratio}$* is the

162 stoichiometric molar C to O_2 ratio (127/175; Broecker et al., 1985).

163 **3. Results**

164 **3.1. Barite is the main carrier of Ba_{xs}**

165 Several barite particles were observed at proximity to biogenic fragments (Fig. 3) suggesting the important role of the

166 biogenic microenvironments in barite formation (Bishop, 1988; Dehairs et al., 1980; Stroobants et al., 1991). However,

167 no barite crystals were observed in surface waters of Station 26 indicating different processes generating high Ba_{xs}

168 concentrations between surface and mesopelagic samples. Indeed, the very high Ba_{xs} concentration in surface waters

169 of Station 26 (Fig. 5) was not related to barite particles but more likely to Ba uptake and adsorption by biota, as reported

170 by Sternberg et al. (2005) in culture experiments. This result fits in the concept of barite formation proposed by

171 Stroobants et al. (1991) showing that the barium sulphate in biogenic aggregates of surface waters is not crystallized

172 whereas below this surface layer, when degradation occurs, the barite is present as micro-particles. In the mesopelagic

173 layer, these micro-sized barite particles are characterized by different shapes and sizes (Fig. 3; Dehairs et al., 1980; S.

174 Jacquet, personal communication).

175 We evaluated the contribution of the barite particles to Ba_{xs} for the sample collected at 600 m of Station 69 (0.003%

176 of the total filter surface was analysed), which was selected because of its high mesopelagic Ba_{xs} content (Fig. 5).

177 Using the Field Emission Scanning Electron Microscope (FE-SEM), we detected the barite particles present in this

178 surface area and determined their volume. To this aim, each barite particle was pictured using a magnification setting

179 between 12,000 and 15,000×. Images were then analysed with the software ImageJ and, for each barite particle, the

180 longest and shortest lengths were measured and converted from pixel to nanometres. Barite particles were then

181 assimilated to ellipses to deduce their volume. Finally, the concentration of pBa in barite particles was calculated using

182 Eq. (3):

$$\text{pBa in barite} = \Sigma \, [V \times \mu_{BaSO4} \times (M_{Ba} / M_{BaSO4}) \,] / V_{SW} \quad (3)$$

184 where V is the volume of each $BaSO_4$ particle (between 0.01 and 3.96 μm^3), μ_{BaSO4} is the density of barite (4.45 g cm^{-}

185 ^{3}), M_{Ba} / M_{BaSO4} is the molar proportion of barium in $BaSO_4$ (0.59) and V_{SW} is the volume of filtered seawater (equivalent

186 to 0.2 mL through this portion of filter). Assuming that this filter portion is representative of the whole filter, the

187 concentration deduced from the FE-SEM reached 1260 pmol L^{-1}. This is in the same order of magnitude that the

188 concentration of total Ba_{xs} analysed by ICP-MS (831 pmol L^{-1}) on the whole filter of this sample. The similarity

189 between both estimations is remarkable considering the limitations of the FE-SEM procedure (i.e. the very small

190 fraction of filter analysed). This also confirms that Ba_{xs} is carried by barite particles in the mesopelagic layer, as

191 observed earlier (Dehairs et al., 1980).

192 ### 3.2. Particulate biogenic Ba_{xs} profiles

193 #### 3.2.1. Section overview

194 The high resolution section of Ba_{xs} concentrations (Fig. 4) shows elevated concentrations in the mesopelagic layer

195 across the section (Ba_{xs} (depth between 100 and 1000 m) = 333 ± 224 pmol L^{-1}; median ± 1s.d.; n=209). In comparison,

196 the surface ocean (depth < 100 m) and the deep ocean (depth > 1000 m) are characterized by lower median values (94

197 and 114 pmol L^{-1}, n=113 and 199, respectively). Exceptions can be observed in the upper waters at Stations 25 and 26

198 and close to the seafloor at Stations 29, 32, 36, 38 and 71, and may be attributed to Ba assimilation by phytoplankton

199 (Stations 25 and 26), and sediment resuspension (Stations 29, 32, 36, 38, 71; Gourain et al., 2017; this issue).

200 Concentrations ranged from 4 (Station 11, 55 m) to 24643 (Station 26, 35 m) pmol L^{-1} in surface waters and from 7

201 (Station 71, 350 m) to 1388 (Station 15, 300 m) pmol L^{-1} in the mesopelagic layer (100–1000 m). In the mesopelagic

202 layer, where the maximum Ba_{xs} concentrations were generally observed, the highest Ba_{xs} concentration was determined

203 in the NAST province, reaching 1388 pmol L^{-1} at 300 m of Station 15. However, these maxima occurred in a relatively

204 narrow depth interval (a layer of 100–300 m), while the maximum were spread over larger depth intervals at other

205 stations, in particular in the ARCT province (layer of the Ba_{xs} maxima: 1200 m at Station 69).

206 #### 3.2.2. Individual Profiles

207 In the following section and if no specific notification are given, only the Ba_{xs} concentrations determined using Niskin

208 bottles are described because of (1) the good comparison between both Niskin and Go-Flo dataset (regression slope:

209 0.94; r²: 71 %; p<0.01; n=91); (2) the better resolution in the 100–1000 m layer for Niskin bottles; and (3) the same

210   cast between Niskin data and 234-Thorium data used for the determination of POC export. A comparison between

211   primary production, POC export and POC remineralisation is addressed in Section 4.4.

212   The vertical profiles of Ba_{xs} concentrations at all stations are shown in Figure 5.

213   In the NAST province (Station 13), the Ba_{xs} concentrations steadily increased from the surface to 400 m, reaching 961

214   pmol L^{-1}, then decreased with depth, reaching the background level of 180 pmol L^{-1} at 1500 m.

215   In the West European basin of the NADR province, vertical profiles of Ba_{xs} were similar, yet concentrations in the

216   mesopelagic layer were smaller at Station 21, as the Ba_{xs} peaked only to 524 pmol L^{-1}. Ba_{xs} concentrations returned to

217   the background value at 1200 m. Ba_{xs} concentration in surface waters of Station 26 were the highest of the entire

218   section, and reached 1888 pmol L^{-1} at 50 m. Below this depth, Ba_{xs} concentrations decreased back to the background

219   level at 100 m, then increased again, with a second peak of 451 pmol L^{-1} at 200 m. In the Icelandic basin of the NADR

220   province, Ba_{xs} concentrations were relatively high, reaching 646 and 711 pmol L^{-1} at 200 m of Station 32 and at 300

221   m of Station 38, respectively. These stations were also characterized by Ba_{xs} profiles displaying a double peak at 200

222   and 450 m for Station 32, and at 300 and 700 m for Station 38. Below this second maximum, Ba_{xs} concentrations

223   decreased to the background level at 1000 m for both stations.

224   In the ARCT province, a similar double peak profile was observed at Station 44, in the Irminger Sea, with Ba_{xs}

225   concentrations reaching 747 pmol L^{-1} at 400 m and 823 pmol L^{-1} at 700 m. Then, Ba_{xs} concentrations returned to the

226   background value at 1100 m. Close to the Greenland margin (Station 51), Ba_{xs} concentrations were lower than at other

227   stations reaching 495 pmol L^{-1} at 300 m, before to decrease until the background level at 1000 m.

228   The Ba_{xs} concentrations of Stations 44 and 51 were compared to those obtained at Station 11 (63.5°N–324.8°E) and

229   Station 5 (56.9°N–317.2°E) of the GEOSECS cruise, in summer 1970 (Brewer et al., unpublished results). The Ba_{xs}

230   concentrations obtained at GEOSECS Station 11 are in similar range as those measured at GEOVIDE Station 44 (173–

231   658 pmol L^{-1} and 116–823 pmol L^{-1}, respectively). Similar ranges were also observed between GEOSECS Station 5

232   and GEOVIDE Station 51 (170–402 pmol L^{-1} and 127–359 pmol L^{-1}, respectively).

233   In the Labrador Sea (Stations 64, 69 and 77), high Ba_{xs} concentrations (> 450 pmol L^{-1} and up to 863 pmol L^{-1} at

234   Station 69) were measured at greater depths than for other stations, and Ba_{xs} concentrations did not return to the

235   background level at 1000–1500 m as observed elsewhere in the section. Samples dedicated to trace metals (Go-Flo

236   sampling) indicated that Ba_{xs} concentrations decreased to the background level (180 pmol L^{-1}) at 1300, 1700 and 1200

237   m for Stations 64, 69 and 77, respectively.

238   ### 3.3. Mesopelagic Ba_{xs}

239   The Ba_{xs} concentrations were integrated (trapezoidal integration) over two depth intervals of the mesopelagic layer

240   (100–500 m and 100–1000 m; Table 2) to obtain a depth-weighted average (DWA) Ba_{xs} values.

241   The DWA Ba_{xs} values between 100 and 500 m ranged from 399 to 672 pmol L^{-1} and from 315 to 727 pmol L^{-1} between

242   100 and 1000 m (Stations 51 and 69, respectively). For both depth intervals, DWA Ba_{xs} values varied by less than a

243   factor of 1.4, being larger for the 100–1000 m interval in the Labrador Sea (Stations 64, 69 and 77). We, thus,

244   considered the 100–1000 m depth interval as the interval representing the best the complete mesopelagic layer.

245   The lowest median DWA Ba_{xs} was observed in the NADR province (403 ± 34 pmol L^{-1} between 100 and 1000 m,

246   n=4), while the highest median DWA Ba_{xs} was observed in the ARCT province (566 ± 155 pmol L^{-1} between 100 and

247   1000 m, n=5). Station 13, in the NAST province, was characterized by a similar DWA Ba_{xs} than those determined

248   within the NADR province, i.e. 419 pmol L^{-1}. In the ARCT province, the DWA Ba_{xs} were variable, ranging from 315

249   pmol L^{-1} at Station 51 to 727 pmol L^{-1} at Station 69, with a high DWA Ba_{xs} of 633 at Station 44.

250   Because of differences in the depths at which the Ba_{xs} signal decreased to the background level, we decided to integrate

251   the Ba_{xs} signal down to 1000 m to enable comparison of the DWA Ba_{xs} values between stations.

252   In a few cases, such as the stations in the Labrador Sea where the background level was not reached at 1000 m, we

253   estimated the DWA Ba_{xs} below 1000 m. However, this modification did not change significantly the magnitude of the

254   DWA Ba_{xs}, with the concentrations integrated over the 100–1300 m (Station 64), 100–1700 m (Station 69) and 100–

255   1200 m (Station 77) being between 1.0 and 1.5 fold lower than for integrations over the 100–1000 m range.

256   **4. Discussion**

257   **4.1. Factors influencing the DWA Ba_{xs} in the North Atlantic**

258   **4.1.1. Influence of the intensity and stage of the bloom**

259   We compared our Ba_{xs} inventories with the averaged biomass development from January to June 2014 (Fig. 6), which

260   is the period integrating the complete productive period in the North Atlantic until our sampling.

261   Along the GEOVIDE transect, the most productive area during this period was clearly the Labrador Sea of the ARCT

262   province, where Chl-*a* concentrations averaged 6 mg m^{-3} (Fig. 6). This basin was sampled during the decline of the

263   bloom (Fig. 1; Chl-*a* concentration was > 3 mg m^{-3} one month before the sampling, and low PP and nutrient

264   concentrations during sampling), which could explain the high DWA Ba_{xs} observed in this area (Table 2). To a lesser

265   extent than the Labrador Sea, the West European basin of the NADR province, and in particular the area around Station

266   21, was characterized by an important biomass level between January and June (Fig. 6). This bloom started in May

267   (Fig. 1; Chl-a concentration ≈ 3 mg m^{-3} one month before the sampling) and was still progressing during the sampling,

268   as indicated by the high PP (135 mmol m^{-2} d^{-1}). These features can explain the lower DWA Ba_{xs} observed at Station

269   21 (Table 2) compared to the Labrador Sea. The other stations of the NADR (Stations 26, 32 and 38) were sampled

270   during the bloom development (Fig. 1 and high PP reaching 174 mmol m^{-2} d^{-1} at Station 26 during sampling) and were

271   characterized by lower DWA Ba_{xs} compared to other stations, suggesting a time lag between production and Ba_{xs}

272   signal. However, this was not the case for Station 44, in the Irminger Sea of the ARCT province, sampled during the

273   bloom (high PP, high Chl-*a* and high nutrient concentrations during the sampling period) and characterized by one of

274   the highest DWA Ba_{xs}. This high Ba_{xs} inventory may reflect an important past bloom, as evidenced in fact by the

275   satellite Chl-*a* data (see Table 2 or Fig. 9 in Lemaitre et al., in prep.), highlighting the patchiness of the phytoplankton

276   blooms in this area.

277   As deduced by different authors, the mesopelagic Ba_{xs} signal is related to a past surface production and builds up

278   during the growth season (Dehairs et al., 1997; Cardinal et al., 2001, 2005). The large regional and temporal variability

279   of the bloom development involves thus a large variability of the mesopelagic Ba_{xs} signal in the North Atlantic.

Biogeosciences
Open Access
Discussions
EGU

4.1.2. Influence of water masses/physical forcing

The largest Ba_{xs} inventory was determined in the Labrador Sea (Stations 64, 69 and 77), characterized by the presence of the Labrador Sea Water (LSW; potential temperature between 2.7 and 3.8 °C and salinity below 34.9; Harvey, 1982; Yashayaev, 2007) in the upper 1500 m. The LSW formation takes place in the central Labrador Sea, where convection reached ~1700 m during the winter preceding GEOVIDE (Fig. 2; Kieke and Yashayaev, 2015). The deepening of the mixed layer depth has been recently shown as a major source (from 23 % to > 100 % in high latitude regions) of organic carbon to the mesopelagic zone (Dall'Olmo et al., 2016), supporting the carbon demand of the mesopelagic food web (Burd et al., 2010; Aristegui et al., 2009). Moreover, the highest mesopelagic prokaryotic heterotrophic abundance during GEOVIDE was observed in the central Labrador Sea (Station 69), reaching 896 cells μL^{-1} at 500 m, while the median values at the other stations for which bacterial cell numbers were available for the mesopelagic zone (Stations 13, 21, 26, 32 and 38), reached 258 ± 60 cells μL^{-1} at the same depth (J. Laroche, J. Ratten and R. Barkhouse, personal communication). Therefore, the LSW subduction area appears to reinforce the microbial loop by increasing the layer in which the bacteria can thrive feeding on increased food supplies. This condition appears to enhance the Ba_{xs} inventory.

The LSW was also present in the Irminger Sea between 500 and 1000 m at Station 44 (Fig. 2), where a second Ba_{xs} peak was observed (823 and 632 pmol L^{-1} at 700 and 800 m; Fig. 5). In the Temperature-Salinity plot, these high Ba_{xs} concentrations are clearly associated with the presence of LSW (Fig. 7a), suggesting that this Ba_{xs} peak could represent an advected signal. At Station 44, the contribution of the advected signal would be about 89 pmol L^{-1} (14 % of the total signal), which is within the uncertainty of the flux. Similarly, a second Ba_{xs} peak was observed at 450 m of Station 32 (Fig. 5) and the Temperature-Salinity plot (Fig. 7b) points out that this second peak was related to the presence of the Subarctic Intermediate water (SAIW; temperature of 5.6 ± 0.1 °C and salinity of 34.70 ± 0.02; Alvarez et al., 2004), which contributes to 14 pmol L^{-1} (3 % of the total signal).

Station 38 was also characterized by a second Ba_{xs} peak at 700 m (Fig. 5), probably unrelated to the presence of a specific water mass since there are no changes in the Temperature-Salinity plot (Fig. 7b). No water masses influence was detected at the remaining stations. Overall, lateral transport influencing the local Ba_{xs} distributions was observed at two stations during GEOVIDE but these did not significantly modify the magnitude of the local mesopelagic Ba_{xs} inventory. However, the subduction occurring in the Labrador Sea resulted in larger mesopelagic DWA Ba_{xs}, probably due to high organic export and associated prokaryotic heterotrophic activity in these areas.

4.1.3. Influence of the phytoplankton community structure

The different Ba_{xs} inventories may also be influenced by the different phytoplankton communities encountered in each province.

The ARCT province was dominated by diatoms (median value: 63 ± 19 % of the total phytoplankton community taxa; Tonnard et al., 2017, this issue) and was characterized by the highest DWA Ba_{xs} values while the NAST and NADR provinces were characterized by higher abundance of haptophytes (median value: 43 ± 16 % of the total phytoplankton community taxa; Tonnard et al., 2017, this issue) and by lower Ba_{xs} inventories. Coccolithophorids are part of the haptophyte family and their dominance was confirmed by visual observations on filters (surface down to 400 m) by FE-SEM. Calcifiers, such as coccolithophorids, have been shown to be more efficient in transferring carbon to the

317   deep ocean compared to diatoms (Francois et al., 2002; Klaas and Archer, 2002; Lam et al., 2011). This difference

318   could result from the low compaction or the high fluffiness of diatom aggregates, the high degree of degradability of

319   organic compounds within diatom aggregates, the greater calcite density, the resistance of calcite to grazing and the

320   more refractory nature of the exported organic matter associated to calcite (Bach et al., 2016; Francois et al., 2002;

321   Klaas and Archer, 2002; Lam et al., 2011; Le Moigne et al., 2013a; Ragueneau et al., 2006). Therefore, enhanced

322   particle degradation when diatoms are predominant seems to increase the mesopelagic DWA Ba_{xs}.

4.2. Relationship between Ba_{xs} and carbon remineralisation in the North Atlantic

324   The mesopelagic Ba_{xs} inventory can be related to the rate of oxygen consumption (JO_2), which can be then converted

325   into a mesopelagic carbon remineralisation (Eq. 2). The relationship between the Ba_{xs} inventory and the JO_2 has been

326   determined in the Southern Ocean (Shopova et al., 1995; Dehairs et al., 1997; Eq. 1), and it is of interest to investigate

327   if this relationship can be applied in the North Atlantic.

328   For this purpose, we have calculated the oxygen utilization rate (OUR; $\mu mol\ kg^{-1}\ yr^{-1}$), which is determined by dividing

329   the apparent oxygen utilization (AOU, in $\mu mol\ kg^{-1}$) by the water mass age (Table S1). From the Iberian coasts to

330   Greenland, the age calculation was based on CFC-12 (when available, otherwise CFC-11) determined in 2012 (OVIDE

331   CARINA cruise, de la Paz et al., 2017). In the Labrador Sea, the mean age of LSW has been estimated by Rhein et al.

332   (2015) based on a 25 year record of CFC contents. The OUR was then integrated over the 100–1000 m layer. The

333   relationships between the Ba_{xs} inventories and the oxygen consumption rates determined using the Southern Ocean

334   equation (Eq. 1) and the one deduced here for the North Atlantic (via the OUR) are compared in Figure 8. This new

335   relationship is significant (p-value = 0.006; Fig. 8) but does not include the Station 44, which was located in the

336   Irminger Gyre (Zunino et al., 2017; this issue). This physical feature may reflect a greater and/or longer mesopelagic

337   Ba_{xs} accumulation in this area explaining the difference compared to other stations.

338   Figure 8 suggests that for a given mesopelagic Ba_{xs} inventory the JO_2 is smaller in the North Atlantic than in the

339   Southern Ocean, with the relationship for the North Atlantic being:

340    $$JO_2 = (\text{mesopelagic } Ba_{xs} - Ba_{\text{residual}}) / 24000 \qquad (4)$$

341   where JO_2 is the rate of oxygen consumption ($\mu mol\ L^{-1}\ d^{-1}$), $mesopelagic\ Ba_{xs}$ is the depth-weighted average in the

342   mesopelagic layer (DWA; $pmol\ L^{-1}$), $Ba_{residual}$ is the deep ocean Ba_{xs} value observed at zero oxygen consumption (or

343   Ba_{xs} background signal; $250\ pmol\ L^{-1}$).

344   However, this new relationship is sensitive to potential errors. The OUR has been shown to under-estimate the ocean

345   respiration because of the non-proportional diffusive mixing of AOU and water mass age resulting in an excess loss

346   of AOU versus age (Koeve and Kähler, 2016). This would decrease the mismatch between the Southern Ocean and

347   North Atlantic regressions. Errors can also be directly associated to the CFC-based age values of the water masses,

348   which would appear especially critical for LSW. Indeed, the severe winter preceding the cruise (2013/2014) appeared

349   to have strongly ventilated LSW with a mixed layer depth exceeding 1700 m (Kieke and Yashayaev, 2015), indicating

350   that the mean age (4 years) estimated by Rhein et al. (2015) may have over-estimated the real LSW age (P. Lherminier,

351   personal communication). Moreover, in the Labrador Sea, the residence time of LSW strongly varies between the

352   central Labrador Sea (4–5 years) and the boundary currents off the Greenland and Newfoundland coasts (a few months;

353   Deshayes et al., 2007; Straneo et al., 2003). The over-estimation of these ages could have directly under-estimate the

354   OUR, resulting, again, to bring more closely together the both North Atlantic and Southern Ocean regressions.

355   In the following discussion, carbon remineralisation fluxes deduced in the North Atlantic (GEOVIDE and GEOSECS

356   cruises) are estimated by using Eq. (4) and (2). These fluxes are compared to carbon mesopelagic remineralisation

357   fluxes calculated with the Ba_{xs} method in the World Ocean (Table 3). Fluxes obtained during GEOVIDE, especially

358   in the ARCT province, were higher than fluxes based on Ba_{xs} data reported for the Southern and Pacific Oceans,

359   highlighting an important remineralisation in the northern part of this basin compared to other oceans.

360   **4.3. Comparison of remineralisation fluxes deduced from different methods**

361   **4.3.1. Remineralisation from direct measurements**

362   In the North Atlantic, carbon respiration rates were also deduced by surface drifting sediment traps and associated-

363   shipboard incubations. Collins et al. (2015) determined very high respiration rates reaching 39 and 72 mmol C m^{-2} d^{-1}

364   at sites located in the NADR and in the ARCT provinces, respectively. Nevertheless, these high fluxes were deduced

365   in the upper mesopelagic layer (50–150 m) where respiration is greater compared to the lower mesopelagic layer (150–

366   1000 m). This different depth interval could thus explain the lower integrated respiration rates determined in our study.

367   Using a similar method supplemented by measurements of zooplankton respiration, Giering et al. (2014) determined

368   respiration rates in the NADR province (PAP site) reaching 7.1 mmol C m^{-2} d^{-1} during summer. This flux, determined

369   over the 50–1000 m depth interval, is in the same order of magnitude than our estimates in the NADR province.

370   **4.3.2. Remineralisation from the deep sediment traps**

371   The remineralisation flux in the mesopelagic layer can also be derived from the difference between a deep POC export

372   flux and a surface POC export flux. Honjo et al. (2008) compiled deep POC export fluxes from moored and time-series

373   sediment traps and calculated the corresponding export production (upper-ocean POC export flux) using an ecosystem

374   model (Laws et al., 2000) for most world provinces. Then, by difference, the authors estimated an annual average of

375   carbon remineralisation fluxes in the mesopelagic layer reaching, after conversion into daily average fluxes, values of

376   34 mmol C m^{-2} d^{-1} in the ARCT province, 9 mmol C m^{-2} d^{-1} in the NADR province and 4 mmol C m^{-2} d^{-1} in the NAST

377   province. Noteworthy, the flux in the ARCT province was the highest mesopelagic remineralisation flux estimated

378   worldwide (with the region around Cape Verde), confirming the important remineralisation in the northern part of the

379   North Atlantic compared to other oceans. The values published by Honjo et al. (2008) for the North Atlantic are

380   relatively similar to the median values obtained during GEOVIDE in each province. Indeed, mesopelagic

381   remineralisation fluxes based on the Ba_{xs} proxy at Station 13 were similar than the value reported by Honjo et al.

382   (2008) for the NAST province, while they were 2 and 4 fold lower in the NADR and in the ARCT provinces,

383   respectively.

384   Overall, the remineralisation fluxes deduced from the Ba_{xs} proxy are in concordance with those obtained by the other

385   methods, confirming the order of magnitude of the mesopelagic remineralisation fluxes determined in this study of the

386   North Atlantic (Fig. 9).

4.4. The biological carbon pump in the North Atlantic

387
388   In order to investigate the efficiency of the biological carbon pump in the North Atlantic, we examined the daily PP
389   (A. Roukaerts, D. Fonseca Batista and F. Deman, unpublished data), the upper-ocean POC export (Lemaitre et al., in
390   prep) and the POC remineralisation in the mesopelagic layer (Table 3; Fig. 10).

391   During GEOVIDE, low (≤ 12 %) export efficiencies (i.e., the ratio between PP and POC export) were observed at most
392   stations indicating an accumulation of biomass in surface waters or a strong turn-over of the exported organic matter
393   due to important remineralisation occurring in the upper water column (< 100 m). Yet, relatively high POC
394   remineralisation fluxes were also measured in the mesopelagic layer, equalling or exceeding the POC export fluxes at
395   some stations. This highlights a strong mesopelagic remineralisation with little or no material left for export to the
396   deep ocean, but above all, it involves an imbalance between carbon supplies and mesopelagic remineralisation.

397   This imbalance can be caused by the distinct time scales over which the PP, POC export and POC remineralisation
398   fluxes operate. Indeed, the measurements of PP represent a snapshot (24h incubations) while measurements of export
399   (^{234}Th) integrate several weeks and remineralisation (Ba_{xs}) integrate probably much longer time scales. Moreover,
400   previous studies in the Southern Ocean showed that mesopelagic processing of exported organic carbon, as reflected
401   by Ba_{xs}, has a phase lag relative to the upper-ocean processes (Dehairs et al., 1997; Cardinal et al., 2005). Thus, we do
402   not expect mesopelagic Ba_{xs} to be in phase with coinciding amplitude of PP and subsequent export. Because of the
403   observed high remineralisation fluxes relative to the export fluxes, particularly in the ARCT province, we suppose that
404   the surface particulate organic matter sank and accumulated in the mesopelagic layer in a period preceding the specific
405   time windows for POC export and PP, leading to an important remineralisation. This can be amplified by the spatial
406   and temporal variability of the phytoplankton bloom in this province, generating sudden high export events and
407   associated remineralisation. Conversely, a fraction of POC, reaching 50% at Station 32, escape remineralisation in the
408   NADR province. The more efficient POC transfer through the mesopelagic layer of this province may be explained by
409   the early sampling compared to the bloom development and/or by the presence of calcified phytoplankton species (see
410   Section 4.1).

411   Overall, the remineralisation in the mesopelagic layer is an important process that needs to be taken into account as
412   our results point to the poor ability of specific areas within the North Atlantic to sequester carbon at depth below 1000
413   m in spring 2014.

5. Conclusion

414
415   We investigated mesopelagic carbon remineralisation fluxes in the North Atlantic during the spring 2014 (GEOVIDE
416   section) using for the first time the particulate biogenic barium inventories measured for this area. The excess barium
417   (Ba_{xs}) content in the mesopelagic layer varied between the different provinces of the North Atlantic. The highest Ba_{xs}
418   inventory was observed in the ARCT province, where high carbon production rates were observed earlier in the season.
419   The regional variations of the Ba_{xs} inventory can also be due to the different phytoplankton community composition
420   encountered along this trans-Atlantic section. Lower contents were determined where the smaller calcified
421   phytoplankton species dominated, as in the NADR province. Finally, the ARCT province was also characterized by
422   an important water mass subduction, generating a larger transport of organic matter to the deep ocean, which might
423   have resulted into an important Ba_{xs} accumulation in the mesopelagic layer.

424   Using the OUR method, we confirmed that mesopelagic Ba_{xs} content can be related to an oxygen consumption, but the

425   relationship between both parameters slightly changed in comparison to the relationship proposed elsewhere for the

426   Southern Ocean. A new relationship is thus proposed for the North Atlantic. This proxy approach provided similar

427   estimations of remineralisation fluxes obtained by independent methods (moored sediment traps, incubations) in the

428   North Atlantic.

429   Overall, in spring 2014, the remineralisation was equal or larger than POC export in the subtropical and subpolar

430   provinces of the North Atlantic, highlighting the important impact of the mesopelagic remineralisation on the

431   biological carbon pump and indicating that little to no POC was transferred below 1000 m in this region.

Acknowledgements

References

448   Alvarez, M., Pérez, F., Bryden, H. and Rios, A. F.: Physical and biogeochemical transports structure in the North
449   Atlantic subpolar gyre, J. Geophys. Res., 109, 1–21, doi:10.1029/2003JC002015, 2004.
450   Aristegui, J., Gasol, J. M., Duarte, C. M. and Herndl, G. J.: Microbial oceanography of the dark ocean' s pelagic realm,
451   Limnol. Oceanogr., 54(5), 1501–1529, 2009.
452   Bach, L. T., Boxhammer, T., Larsen, A., Hildebrandt, N., Schulz, K. G. and Riebesell, U.: Influence of plankton
453   community structure on the sinking velocity of marine aggregates, Global Biogeochem. Cycles, 30, 1145–1165,
454   doi:10.1002/2016GB005372, 2016.
455   Baltar, F., Aristegui, J., Gasol, J. M., Sintes, E. and Herndl, G. J.: Evidence of prokaryotic metabolism on suspended
456   particulate organic matter in the dark waters of the subtropical North Atlantic, Limnol. Oceanogr., 54(1), 182–193,
457   2009.
458   Bishop, J. K. B.: The barite-opal-organic carbon association in oceanic particulate matter, Nature, 332(6162), 341–
459   343, doi:10.1038/332341a0, 1988.
460   Broecker, W. S., Takahashi, T. and Takahashi, T.: Source and flow patterns of deep ocean, J. Geophys. Res., 90, 6925–
461   6939, doi:10.1029/JC090iC04p06925, 1985.
462   Buesseler, K. O. and Boyd, P. W.: Shedding light on processes that control particle export and flux attenuation in the
463   twilight zone of the open ocean, Limnol. Oceanogr., 54(4), 1210–1232, doi:10.4319/lo.2009.54.4.1210, 2009.
464   Buesseler, K. O., Bacon, M. P., Kirk Cochran, J. and Livingston, H. D.: Carbon and nitrogen export during the JGOFS
465   North Atlantic Bloom experiment estimated from 234Th: 238U disequilibria, Deep Sea Res. Part A. Oceanogr. Res.

466   Pap., 39(7–8), 1115–1137, doi:10.1016/0198-0149(92)90060-7, 1992.

467   Buesseler, K. O., Lamborg, C. H., Boyd, P. W., Lam, P. J., Trull, T. W., Bidigare, R. R., Bishop, J. K. B., Casciotti,
468   K. L., Dehairs, F., Elskens, M., Honda, M., Karl, D. M., Siegel, D. a, Silver, M. W., Steinberg, D. K., Valdes, J., Mooy,
469   B. Van and Wilson, S.: Revisiting Carbon Flux Through the Ocean ' s Twilight Zone, Science (80-.)., 316(April),
470   567–570, doi:10.1126/science.1137959, 2007.

471   Burd, A. B., Hansell, D. A., Steinberg, D. K., Anderson, T. R., Aristegui, J., Baltar, F., Beaupré, S. R., Buesseler, K.
472   O., DeHairs, F., Jackson, G. A., Kadko, D. C., Koppelmann, R., Lampitt, R. S., Nagata, T., Reinthaler, T., Robinson,
473   C., Robison, B. H., Tamburini, C. and Tanaka, T.: Assessing the apparent imbalance between geochemical and
474   biochemical indicators of meso- and bathypelagic biological activity: What the @$#! is wrong with present
475   calculations of carbon budgets?, Deep Sea Res. Part II Top. Stud. Oceanogr., 57(16), 1557–1571,
476   doi:10.1016/j.dsr2.2010.02.022, 2010.

477   Burd, A. B., Buchan, A., Church, M., Landry, M. R., McDonnell, A. M. P., Passow, U., Steinberg, D. K. and Benway,
478   H.: Towards a transformative understanding of the ocean' s biological pump: Priorities for future research, Rep. NSF
479   Biol. Biol. Pump Work., (1–67), doi:10.1575/1912/8263, 2016.

480   Cao, Z., Siebert, C., Hathorne, E. C., Dai, M. and Frank, M.: Constraining the oceanic barium cycle with stable barium
481   isotopes, Earth Planet. Sci. Lett., 434, 1–9, doi:10.1016/j.epsl.2015.11.017, 2016.

482   Cardinal, D., Dehairs, F., Cattaldo, T. and André, L.: Geochemistry of suspended particles in the Subantarctic and
483   Polar Frontal zones south of Australia: Constraints on export and advection processes, J. Geophys. Res., 106, 31637,
484   doi:10.1029/2000JC000251, 2001.

485   Cardinal, D., Savoye, N., Trull, T. W., André, L., Kopczynska, E. E. and Dehairs, F.: Variations of carbon
486   remineralisation in the Southern Ocean illustrated by the Baxs proxy, Deep Sea Res. Part I Oceanogr. Res. Pap., 52(2),
487   355–370, doi:10.1016/j.dsr.2004.10.002, 2005.

488   Collier, R. and Edmond, J.: The trace element geochemistry of marine biogenic particulate matter, Prog. Oceanogr.,
489   13, 113–199, 1984.

490   Collins, J. R., Edwards, B. R., Thamatrakoln, K., Ossolinski, J. E., Ditullio, G. R., Bidle, K. D., Doney, S. C. and
491   Mooy, B. A. S. Van: The multiple fates of sinking particles in the North Atlantic Ocean, Global Biogeochem. Cycles,
492   29, 1471–1494, doi:10.1002/2014GB005037, 2015.

493   Dall'Olmo, G., Dingle, J., Polimene, L., Brewin, R. J. W. and Claustre, H.: Substantial energy input to the mesopelagic
494   ecosystem from the seasonal mixed-layer pump, Nat. Geosci., 1(September), 1–6, doi:10.1038/NGEO2818, 2016.

495   Daniault, N., Mercier, H., Lherminier, P., Sarafanov, A., Falina, A., Zunino, P., Pérez, F. F., Ríos, A. F., Ferron, B.,
496   Huck, T., Thierry, V. and Gladyshev, S.: The northern North Atlantic Ocean mean circulation in the early 21st century,
497   Prog. Oceanogr., 146(July), 142–158, doi:10.1016/j.pocean.2016.06.007, 2016.

498   Dehairs, F., Chesselet, R. and Jedwab, J.: Discrete suspended particles of barite and the barium cycle in the open ocean,
499   Earth Planet. Sci. Lett., 49, 528–550, 1980.

500   Dehairs, F., Shopova, D., Ober, S., Veth, C. and Goeyens, L.: Particulate barium stocks and oxygen consumption in
501   the Southern Ocean mesopelagic water column during spring and early summer: Relationship with export production,
502   Deep Sea Res. Part II Top. Stud. Oceanogr., 44(1–2), 497–516, doi:10.1016/S0967-0645(96)00072-0, 1997.

503   Dehairs, F., Jacquet, S., Savoye, N., Van Mooy, B. a S., Buesseler, K. O., Bishop, J. K. B., Lamborg, C. H., Elskens,
504   M., Baeyens, W., Boyd, P. W., Casciotti, K. L. and Monnin, C.: Barium in twilight zone suspended matter as a potential
505   proxy for particulate organic carbon remineralization: Results for the North Pacific, Deep Sea Res. Part II Top. Stud.
506   Oceanogr., 55(14–15), 1673–1683, doi:10.1016/j.dsr2.2008.04.020, 2008.

507   Deshayes, J., Frankignoul, C. and Drange, H.: Formation and export of deep water in the Labrador and Irminger Seas
508   in a GCM, Deep Sea Res. Part I Oceanogr. Res. Pap., 54, 510–532, doi:10.1016/j.dsr.2006.12.014, 2007.

509   Fernández-castro, B., Arístegui, J., Anderson, L., Montero, M. F., Hernández-León, S., Maranon, E. and Mourino-
510   Carballido, B.: Mesopelagic respiration near the ESTOC (European Station for Time-Series in the Ocean, 15.5°W,
511   29.1°N) site inferred from a tracer conservation model, Deep Sea Res. Part I Oceanogr. Res. Pap., 115, 63–73,
512   doi:10.1016/j.dsr.2016.05.010, 2016.

513   Francois, R., Honjo, S., Krishfield, R. and Manganini, S.: Factors controlling the flux of organic carbon to the
514   bathypelagic zone of the ocean, Global Biogeochem. Cycles, 16(4), 1–20, doi:10.1029/2001GB001722, 2002.

515   Ganeshram, R. S., François, R., Commeau, J. and Brown-Leger, S. L.: An experimental investigation of barite
516   formation in seawater, Geochim. Cosmochim. Acta, 67(14), 2599–2605, doi:10.1016/S0016-7037(03)00164-9, 2003.

517   García-Ibáñez, M. I., Pardo, P. C., Carracedo, L. I., Mercier, H., Lherminier, P., Ríos, A. F. and Pérez, F. F.: The water
518   mass structure and transports in the Atlantic Subpolar Gyre, Prog. Oceanogr., 135, 18–36,
519   doi:10.1016/j.pocean.2015.03.009, 2015.

520   Giering, S. L. C., Sanders, R., Lampitt, R. S., Anderson, T. R., Tamburini, C., Boutrif, M., Zubkov, M. V, Marsay, C.
521   M., Henson, S. A., Saw, K., Cook, K. and Mayor, D. J.: Reconciliation of the carbon budget in the ocean's twilight

522 zone, Nature, 507(7493), 480–483, doi:10.1038/nature13123, 2014.
523 Gonzalez-Munoz, M. T., Fernandez-Luque, B., Martínez-Ruiz, F., Chekroun, K. Ben, Arias, J. M., Rodríguez-Gallego,
524 M., Martínez-Canamero, M., de Linares, C. and Paytan, A.: Precipitation of barite by Myxococcus xanthus: possible
525 implications for the biogeochemical cycle of barium, Appl. Environ. Microbiol., 69(9), 5722–5725,
526 doi:10.1128/AEM.69.9.5722, 2003.
527 Gourain, A., Planquette, H., Cheize, M., Menzel, J.-L., Boutorh, J., Shelley, R., Pereira Contraira, L., Lemaitre, N.,
528 Lacan, F., Lherminier, P. and Sarthou, G.: Particulate trace metals along the GEOVIDE section, Biogeosciences, 2017.
529 Harvey, J.: 0-S relationships and water masses in the eastern North Atlantic, Deep Sea Res. Part A. Oceanogr. Res.
530 Pap., 29(8), 1021–1033, 1982.
531 Henson, S. A., Dunne, J. P. and Sarmiento, J. L.: Decadal variability in North Atlantic phytoplankton blooms, J.
532 Geophys. Res., 114(C4), C04013–C04013, doi:10.1029/2008JC005139, 2009.
533 Herndl, G. J. and Reinthaler, T.: Microbial control of the dark end of the biological pump, Nat. Geosci., 6(9), 718–
534 724, doi:10.1038/ngeo1921, 2013.
535 Honjo, S. and Manganini, S. J.: Annual biogenic particle fluxes to the interior of the North Atlantic Ocean; studied at
536 34°N 21°W and 48°N 21°W, Deep Sea Res. Part I Oceanogr. Res. Pap., 40(1), 587–607, 1993.
537 Honjo, S., Manganini, S. J., Krishfield, R. A. and Francois, R.: Particulate organic carbon fluxes to the ocean interior
538 and factors controlling the biological pump: A synthesis of global sediment trap programs since 1983, Prog. Oceanogr.,
539 76(3), 217–285, doi:10.1016/j.pocean.2007.11.003, 2008.
540 Horner, T. J., Kinsley, C. W. and Nielsen, S. G.: Barium-isotopic fractionation in seawater mediated by barite cycling
541 and oceanic circulation, Earth Planet. Sci. Lett., 430, 511–522, doi:10.1016/j.epsl.2015.07.027, 2015.
542 Jacquet, S. H. M., Savoye, N., Dehairs, F., Strass, V. H. and Cardinal, D.: Mesopelagic carbon remineralization during
543 the European Iron Fertilization Experiment, Global Biogeochem. Cycles, 22(1), 1–9, doi:10.1029/2006GB002902,
544 2008a.
545 Jacquet, S. H. M., Dehairs, F., Savoye, N., Obernosterer, I., Christaki, U., Monnin, C. and Cardinal, D.: Mesopelagic
546 organic carbon remineralization in the Kerguelen Plateau region tracked by biogenic particulate Ba, Deep Sea Res.
547 Part II Top. Stud. Oceanogr., 55(5–7), 868–879, doi:10.1016/j.dsr2.2007.12.038, 2008b.
548 Jacquet, S. H. M., Dehairs, F., Dumont, I., Becquevort, S., Cavagna, A.-J. and Cardinal, D.: Twilight zone organic
549 carbon remineralization in the Polar Front Zone and Subantarctic Zone south of Tasmania, Deep Sea Res. Part II Top.
550 Stud. Oceanogr., 58(21–22), 2222–2234, doi:10.1016/j.dsr2.2011.05.029, 2011.
551 Jacquet, S. H. M., Dehairs, F., Cavagna, A. J., Planchon, F., Monin, L., André, L., Closset, I. and Cardinal, D.: Early
552 season mesopelagic carbon remineralization and transfer efficiency in the naturally iron-fertilized Kerguelen area,
553 Biogeosciences, 12, 1713–1731, doi:10.5194/bg-12-1713-2015, 2015.
554 Kieke, D. and Yashayaev, I.: Studies of Labrador Sea Water formation and variability in the subpolar North Atlantic
555 in the light of international partnership and collaboration, Prog. Oceanogr., 132, 220–232,
556 doi:10.1016/j.pocean.2014.12.010, 2015.
557 Klaas, C. and Archer, D. E.: Association of sinking organic matter with various types of mineral ballast in the deep
558 sea: Implications for the rain ratio, Global Biogeochem. Cycles, 16(4), 1–14, doi:10.1029/2001GB001765, 2002.
559 Koeve, W. and Kähler, P.: Oxygen utilization rate (OUR) underestimates ocean respiration: a model study, Global
560 Biogeochem. Cycles, 30, 1166–1182, doi:10.1002/2015GB005354, 2016.
561 de la Paz, M., García-Ibáñez, M. I., Steinfeldt, R., Ríos, A. F. and Pérez, F. F.: Ventilation versus biology: What is the
562 controlling mechanism of nitrous oxide distribution in the North Atlantic?, Global Biogeochem. Cycles, 31(4), 745–
563 760, doi:10.1002/2016GB005507, 2017.
564 Lam, P. J., Doney, S. C. and Bishop, J. K. B.: The dynamic ocean biological pump: Insights from a global compilation
565 of particulate organic carbon, CaCO3, and opal concentration profiles from the mesopelagic, Global Biogeochem.
566 Cycles, 25(3), 1–14, doi:10.1029/2010GB003868, 2011.
567 Lampitt, R. S. and Antia, A. N.: Particle flux in deep seas: Regional characteristics and temporal variability, Deep Sea
568 Res. Part I Oceanogr. Res. Pap., 44(8), 1377–1403, 1997.
569 Laws, E. A., Ducklow, H. and McCarthy, J. J.: Temperature effects on export production in the open ocean, Global
570 Biogeochem. Cycles, 14(4), 1231–1246, doi:10.1029/1999GB001229, 2000.
571 Lemaitre, N., Planquette, H., Dehairs, F., Sarthou, G., Fonseca-Batista, D., Roukaerts, A., Deman, F. and Planchon,
572 F.: High variability of particulate organic carbon export fluxes along the North Atlantic GEOTRACES section GA01.,
573 in prep.
574 Longhurst, A.: Seasonal cycles of pelagic production and consumption, Prog. Oceanogr., 36(95), 77–167, 1995.
575 Martin, J. H., Knauer, G. a., Karl, D. M. and Broenkow, W. W.: VERTEX: carbon cycling in the northeast Pacific,
576 Deep Sea Res. Part A. Oceanogr. Res. Pap., 34(2), 267–285, doi:10.1016/0198-0149(87)90086-0, 1987.
577 Le Moigne, F. A. C., Gallinari, M., Laurenceau, E. and De La Rocha, C. L.: Enhanced rates of particulate organic

578   matter remineralization by microzooplankton are diminished by added ballast minerals, Biogeosciences, 10(9), 5755–
579   5765, doi:10.5194/bg-10-5755-2013, 2013a.
580   Le Moigne, F. A. C., Villa-Alfageme, M., Sanders, R. J., Marsay, C., Henson, S. and García-Tenorio, R.: Export of
581   organic carbon and biominerals derived from 234Th and 210Po at the Porcupine Abyssal Plain, Deep Sea Res. Part I
582   Oceanogr. Res. Pap., 72(August), 88–101, doi:10.1016/j.dsr.2012.10.010, 2013b.
583   Planchon, F., Cavagna, A.-J., Cardinal, D., André, L. and Dehairs, F.: Late summer particulate organic carbon export
584   and twilight zone remineralisation in the Atlantic sector of the Southern Ocean, Biogeosciences, 10(2), 803–820,
585   doi:10.5194/bg-10-803-2013, 2013.
586   Planquette, H. and Sherrell, R. M.: Sampling for particulate trace element determination using water sampling bottles:
587   methodology and comparison to in situ pumps, Limnol. Oceanogr. Methods, 10, 367–388,
588   doi:10.4319/lom.2012.10.367, 2012.
589   Pommier, J., Gosselin, M. and Michel, C.: Size-fractionated phytoplankton production and biomass during the decline
590   of the northwest Atlantic spring bloom, J. Plankton Res., 31(4), 429–446, doi:10.1093/plankt/fbn127, 2009.
591   Ragueneau, O., Schultes, S., Bidle, K., Claquin, P. and Moriceau, B.: Si and C interactions in the world ocean:
592   Importance of ecological processes and implications for the role of diatoms in the biological pump, Global
593   Biogeochem. Cycles, 20(4), n/a-n/a, doi:10.1029/2006GB002688, 2006.
594   Reinthaler, T., van Aken, H., Veth, C., Aristegui, J., Robinson, C., Williams, P. J. B., Lebaron, P. and Herndl, G. J.:
595   Prokaryotic respiration and production in the meso- and bathypelagic realm of the eastern and western North Atlantic
596   basin, Limnol. Oceanogr., 51(3), 1262–1273, 2006.
597   Rhein, M., Kieke, D. and Steinfeldt, R.: Advection of North Atlantic Deep Water from the Labrador Sea to the southern
598   hemisphere, J. Geophys. Res., 120, 2471–2487, doi:10.1002/2014JC010605, 2015.
599   Sanders, R., Henson, S. A., Koski, M., La, C. L. De, Painter, S. C., Poulton, A. J., Riley, J., Salihoglu, B., Visser, A.,
600   Yool, A., Bellerby, R. and Martin, A. P.: The Biological Carbon Pump in the North Atlantic, Prog. Oceanogr., 129,
601   200–218, doi:10.1016/j.pocean.2014.05.005, 2014.
602   Shopova, D., Dehairs, F. and Baeyens, W.: A simple model of biogeochemical element distribution in the oceanic
603   water column, J. Mar. Syst., 6, 331–344, 1995.
604   Sternberg, E., Tang, D., Ho, T. Y., Jeandel, C. and Morel, F. M. M.: Barium uptake and adsorption in diatoms,
605   Geochim. Cosmochim. Acta, 69(11), 2745–2752, doi:10.1016/j.gca.2004.11.026, 2005.
606   Straneo, F., Pickart, R. S. and Lavender, K.: Spreading of Labrador sea water: an advective-diffusive study based on
607   Lagrangian data, Deep Sea Res. Part A. Oceanogr. Res. Pap., 50, 701–719, doi:10.1016/S0967-0637(03)00057-8,
608   2003.
609   Stroobants, N., Dehairs, F., Goeyens, L., Vanderheijden, N. and Van Grieken, R.: Barite formation in the Southern
610   Ocean water, Mar. Chem., 35(1–4), 411–421, doi:10.1016/S0304-4203(09)90033-0, 1991.
611   Taylor, S. R. and Mclennan, S. M.: The continental crust: its composition and evolution, Blackwells., 1985.
612   Tonnard, M., Donval, A., Lampert, L., Claustre, H., Ras, J., Dimier, C., Sarthou, G., Planquette, H., van der Merwe,
613   P., Boutorh, J., Cheize, M., Menzel, J.-L., Pereira Contraira, L., Shelley, R., Bowie, A. R., Tréguer, P., Gallinari, M.,
614   Duprez de Gesincourt, F., Germain, Y. and Lherminier, P.: Phytoplankton assemblages along the GEOVIDE section
615   (GEOTRACES section GA01) using CHEMTAX, Biogeosciences, 2017.
616   Yashayaev, I.: Hydrographic changes in the Labrador Sea, 1960-2005, Prog. Oceanogr., 73, 242–276,
617   doi:10.1016/j.pocean.2007.04.015, 2007.
618   Zunino, P., Lherminier, P., Mercier, H., Daniault, N. and Isabel, M.: The GEOVIDE cruise in May-June 2014 reveals
619   an intense Meridional Overturning Circulation over a cold and fresh subpolar North Atlantic, Biogeosciences, 2017.
620

621

Biogeosciences
Discussions

Open Access

EGU

622 **Table 1:** **Particulate Barium (Ba) and Aluminium (Al) concentrations and resulting recoveries (bold and italic percentages)**
623 **of the certified reference materials SLRS-5 (river water), BHVO-1 (basalt powder), JB-3 (basalt powder) and JGb-1 (gabbro**
624 **powder).**

625

	Ba	Al
SLRS-5 (µg kg^{-1})	13 ± 1	47 ± 2
n=4	95 %	95 %
BHVO-1 (µg g^{-1})	129 ± 1	70118 ± 984
n=4	93 %	96 %
JB-3 (µg g^{-1})	229 ± 13	92144 ± 1620
n=4	94 %	101 %
JGb-1 (µg g^{-1})	68 ± 15	91491 ± 732
n=4	106 %	99 %

626

627

628

629

630

631

632

633

634

635

636

637

638

639

640

641

642

643   **Table 2: Depth-weighted average (DWA) values of mesopelagic Ba$_{xs}$ (in pmol L^{-1}) integrated between 100–500 m and 100–**
644   **1000 m depths. The biogeochemical provinces defined by Longhurst et al. (1995) are also indicated: NAST: North Atlantic**
645   **subtropical gyre; NADR: North Atlantic drift; ARCT: Atlantic Arctic.**

646

647

Province	Station	Latitude (° N)	Longitude (° E)	DWA Ba$_{xs}$ 100-500 m (pmol L^{-1})			DWA Ba$_{xs}$ 100-1000 m (pmol L^{-1})		
NAST	13	41.4	-13.9	578	±	89	419	±	71
NADR	21	46.5	-19.7	428	±	69	394	±	64
	26	50.3	-22.6	405	±	59	391	±	58
	32	55.5	-26.7	522	±	81	413	±	66
	38	58.8	-31.3	572	±	86	465	±	78
ARCT	44	59.6	-38.9	678	±	104	633	±	98
	51	59.8	-42	399	±	72	315	±	58
	64	59.1	-46.1	464	±	95	566	±	99
	69	55.8	-48.1	672	±	111	727	±	118
	77	53	-51.1	472	±	80	505	±	83

648

Biogeosciences Discussions — Open Access — EGU

649
650 **Table 3:** Comparison of the Ba_{xs} inventory (pmol L^{-1}) and related-carbon mesopelagic remineralisation fluxes (mmol C m^{-2} d^{-1}) obtained in the world's ocean.

Cruise (season)	Location	Features	depth interval, m	DWA Ba_{xs} pmol L^{-1}	MR fluxes mmol C m^{-2} d^{-1}	Reference
CLIVAR SR3 - SAZ298 (spring/summer)	Southern Ocean	spring / summer	150 - 400	235 - 554 / 296 - 353	0.3 - 3.0 / 0.2 - 3.4	Cardinal et al., 2005
VERTIGO (summer)	Pacific Ocean	oligotrophic (Aloha station) / mesotrophic (K2 station)	150 - 500	157 - 205 / 367 - 713	1.0 - 3.0 / 2.7 - 8.8	Dehairs et al., 2008
EIFEX (summer)	Southern Ocean	fertilized (in patch) / HNLC (out patch)	150 - 1000	273 - 415 / 233 - 423	2.6 - 7.7 / 1.2 - 8.0	Jacquet et al., 2008a
KEOPS (summer)	Southern Ocean	fertilized (A3 station) / HNLC (C11 station)	125 - 450	342 - 401 / 309 - 493	2.1 - 2.8 / 1.7 - 4.0	Jacquet et al., 2008b
SAZ-SENSE (summer)	Southern Ocean	fertilized (SAZ east) / HNLC (SAZ west)	100 - 600	244 - 395 / 199 - 249	3.0 - 6.1 / 2.1 - 3.1	Jacquet et al., 2011
Bonus GoodHope (summer)	Southern Ocean	North of PF / South of PF	125 - 600	284 - 497 / 235 - 277	2.1 - 6.4 / 1.1 - 1.9	Planchon et al., 2013
KEOPS 2 (spring)	Southern Ocean	fertilized (A3 station) / HNLC (R2 station)	150 - 400	267 - 314 / 572	0.9 - 1.2 / 4.2	Jacquet et al., 2015
GEOSECS II (summer)	North Atlantic	NAST+NADR / ARCT	100 - 1000	199 - 361 / 242 - 413	0.5 - 4.9 / 1.7 - 6.3	Brewer (unpublished values)
GEOVIDE (spring)	**North Atlantic**	**NAST (station 13)**	**100 - 1000**	**419**	**4.6**	**this study**
		NADR (station 21)		**394**	**3.9**	
		NADR (station 26)		**391**	**3.8**	
		NADR (station 32)		**413**	**4.4**	
		NADR (station 38)		**465**	**5.9**	
		ARCT (station 44)		**633**	**10**	
		ARCT (station 51)		**315**	**1.8**	
		ARCT (station 64)		**566**	**8.6**	
		ARCT (station 69)		**727**	**13**	
		ARCT (station 77)		**505**	**6.9**	

651

652 **Table 4: Comparison of the mesopelagic POC remineralisation fluxes (Remineralisation) with primary production (PP)**
653 **and POC export fluxes in the upper water column (Export). All fluxes are expressed in mmol C m⁻² d⁻¹. [1] PP data from**
654 **A. Roukaerts, D. Fonseca Batista and F. Deman (unpublished data); [2] Export data from Lemaitre et al. (in prep.).**
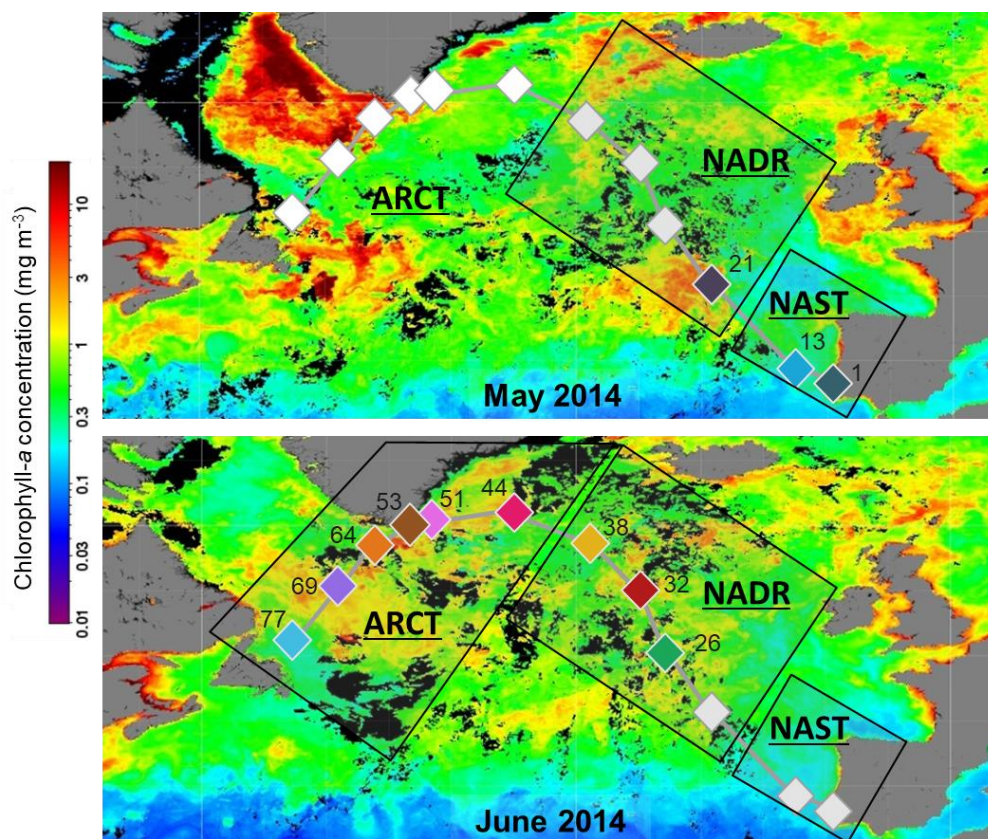
655

Station	ARCT - Labrador Sea			ARCT - Irminger Sea			NADR			NAST
	77	69	64	51	44	38	32	26	21	13
PP [1]	95	31	67	165	137	68	142	174	135	80
Export [2]	6	10	8	3	1	5	8	7	5	2
Remineralisation	7	13	9	2	10	6	4	4	4	5

656

657

658

659

660

Figure 1: Satellite Chlorophyll-a concentrations (MODIS Aqua from http://oceancolor.gsfc.nasa.gov), in mg m^{-3} during the GEOVIDE cruise (May and June 2014). The province are indicated: NAST: North Atlantic Subtropical gyre; NADR: North Atlantic Drift; ARCT: Atlantic Arctic. Diamonds indicate stations, coloured according to their approximate time of sampling.
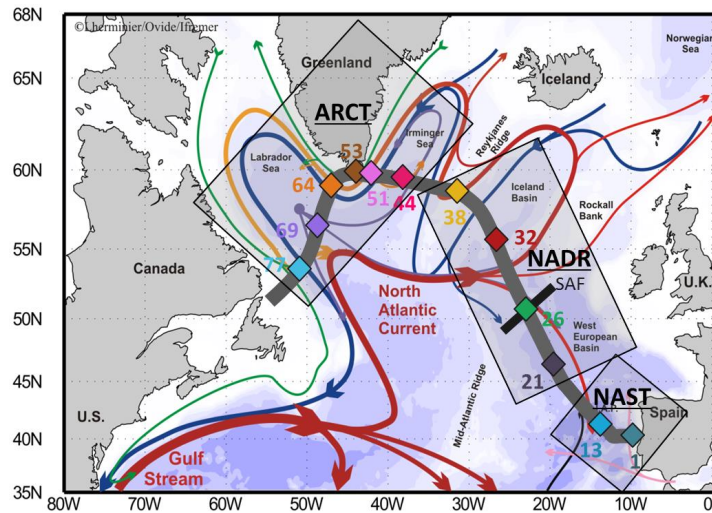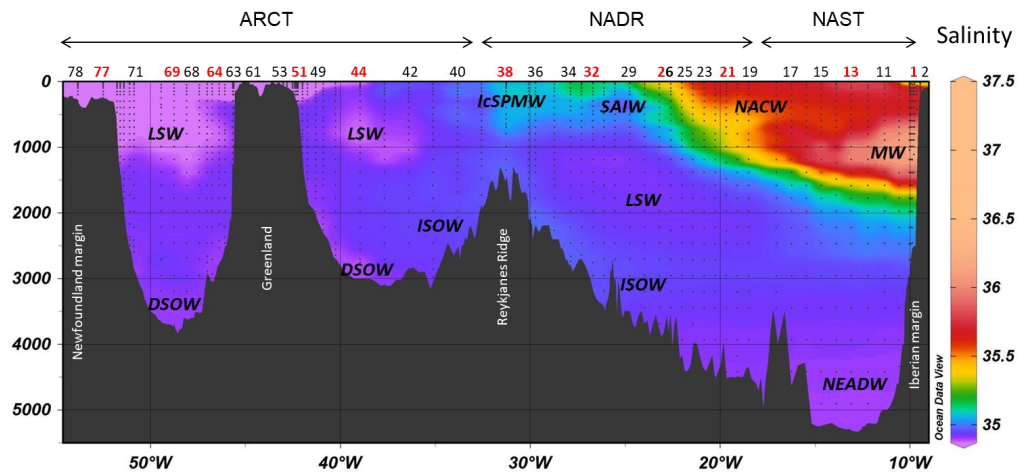
665

666

667

668

669

670

671

672

673

674   **(a)**

675

676   **(b)**

677

678   **Figure 2:** **(a) Schematic of the circulation features, adapted from García-Ibáñez et al. (2015). Bathymetry is plotted in**
679   **colour with colour change at 100 m, at 1000 m and every 1000 m below 1000 m. The red and green arrows represent**
680   **the main surface currents, the pink and orange arrows represent the intermediate currents and the blue and purple**
681   **arrows represent the deep currents. (b) Salinity along the GEOVIDE section, and associated water masses: LSW:**
682   **Labrador Sea Water; ISOW: Iceland–Scotland Overflow Water; IcSPMW: Iceland Subpolar Mode Water; SAIW:**
683   **Subarctic Intermediate Water; NACW: North Atlantic Central Waters; MW: Mediterranean Water; DSOW: Denmark**
684   **Strait Overflow Water; NEADW: North East Atlantic Deep Water. Stations in red correspond to stations where detailed**
685   **vertical Niskin profiles were collected. In both figures, the provinces are also indicated: NAST: North Atlantic**
686   **Subtropical gyre; NADR: North Atlantic Drift; ARCT: Atlantic Arctic.**
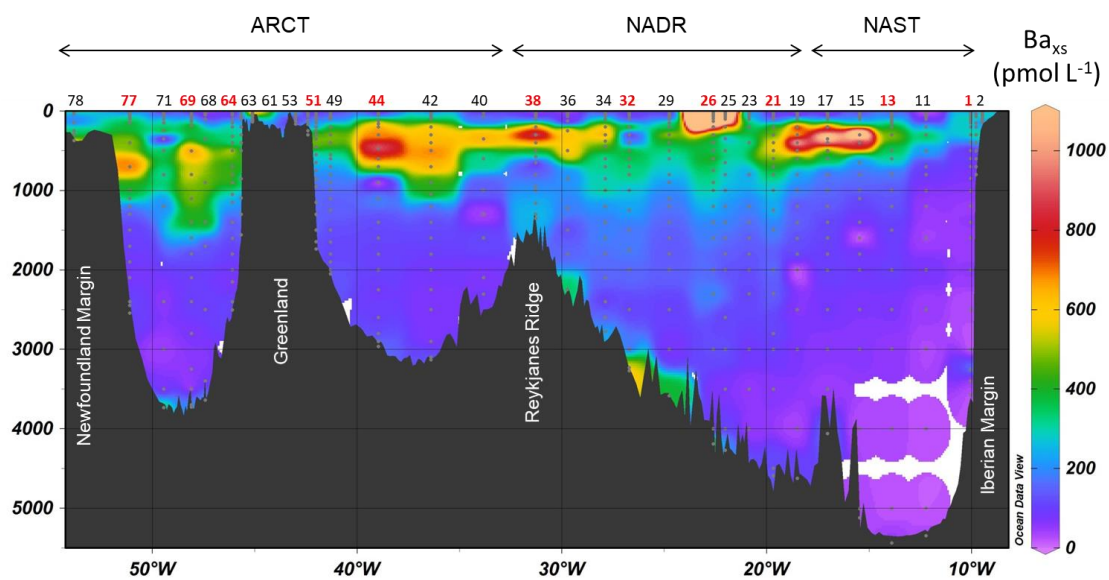
687
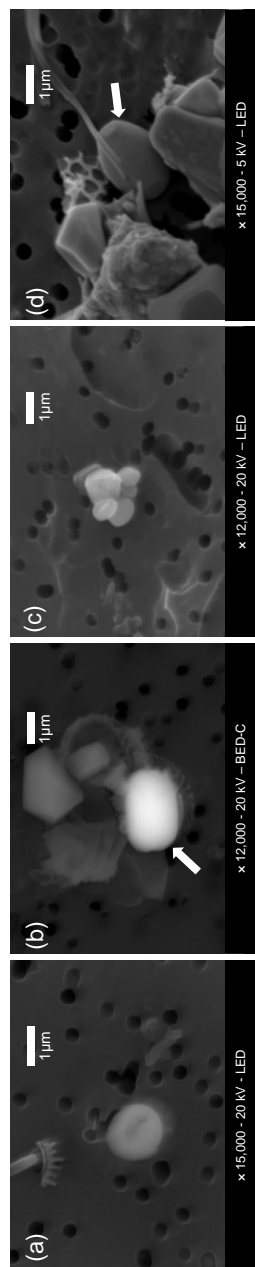
Figure 3: Barite particles observed by FE-SEM at (a) Station 38 (300 m); (b) Station 44 (700 m); (c and d) Station 69 (600 m). White arrows indicate the position of barite crystals.
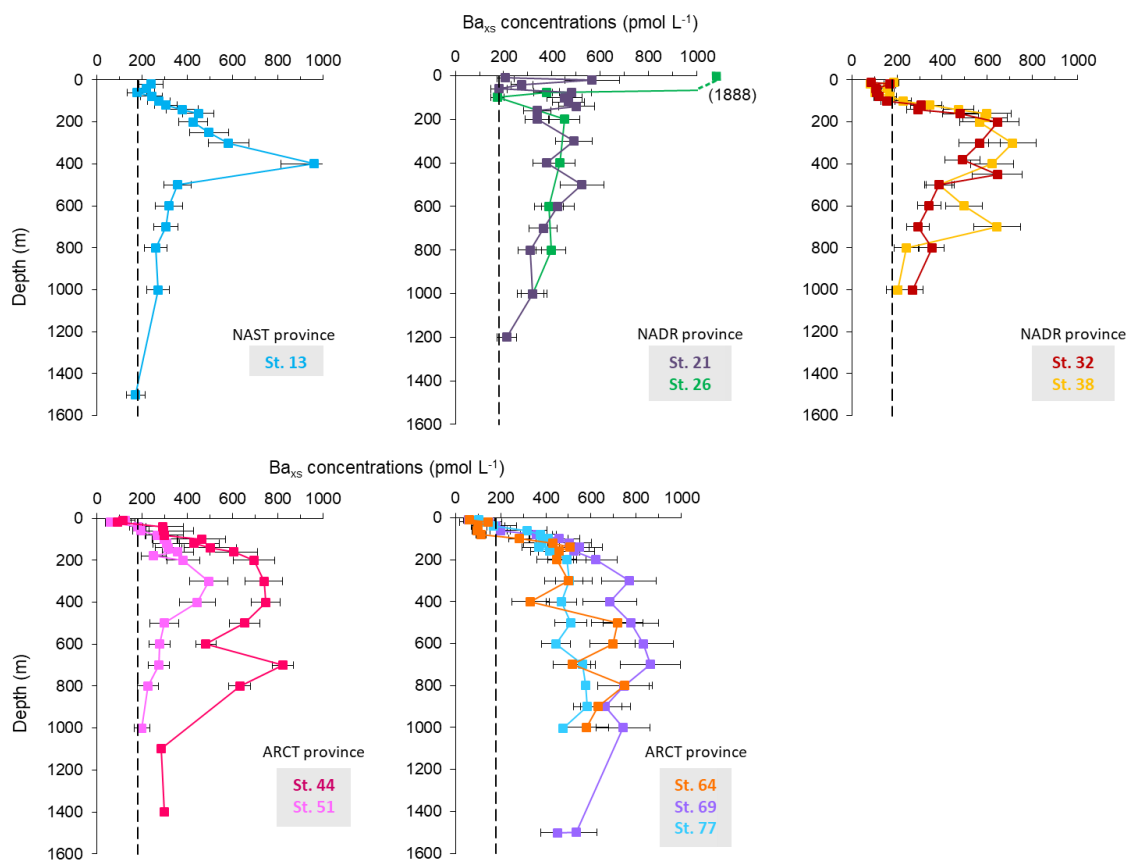
699

Figure 4: Section of the particulate biogenic barium (Ba$_{xs}$) in pmol L^{-1} determined in samples collected with the Go-Flo bottles. Stations in red are those where profiles were obtained from Niskin-rosette sampling.
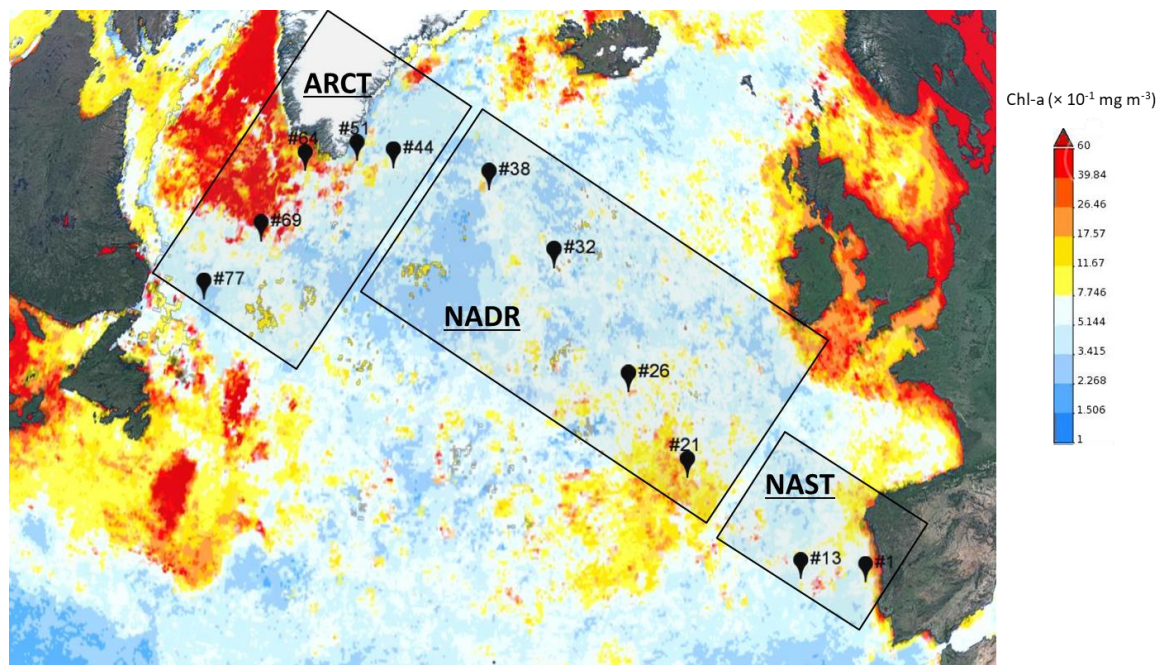
700

701

702

703

Figure 5: Individual profiles of Ba_{xs} concentrations (in pmol L^{-1}) determined using Niskin bottles.

706

Figure 6: Time averaged map of Chlorophyll-a concentrations (in mg m⁻³) over January–June 2014 (monthly 4 km MODIS
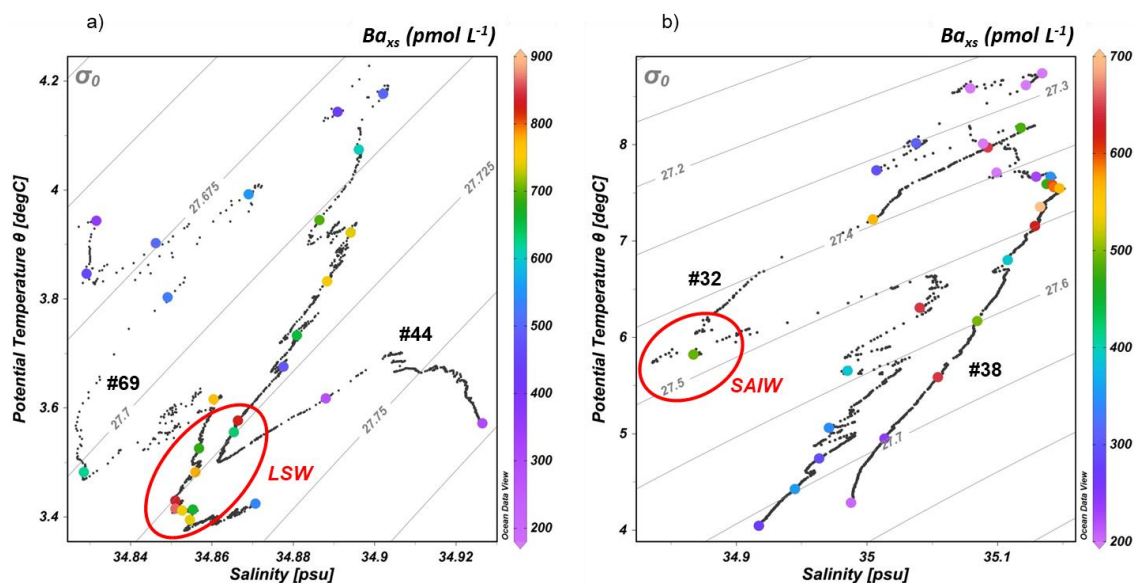Aqua model; http://giovanni.sci.gsfc.nasa.gov/).

707
708

709

710

711
712

713

714

715

Figure 7: Potential temperature θ - salinity plots for the Stations (a) #44 and #69 and (b) #32 and #38 of the GEOVIDE cruise focus on the 50–2000 m depth interval. The concentrations of Ba$_{xs}$ are shown by the coloured points. Isopycnals are also represented. LSW: Labrador Sea Water; SAIW: Subarctic Intermediate Water.
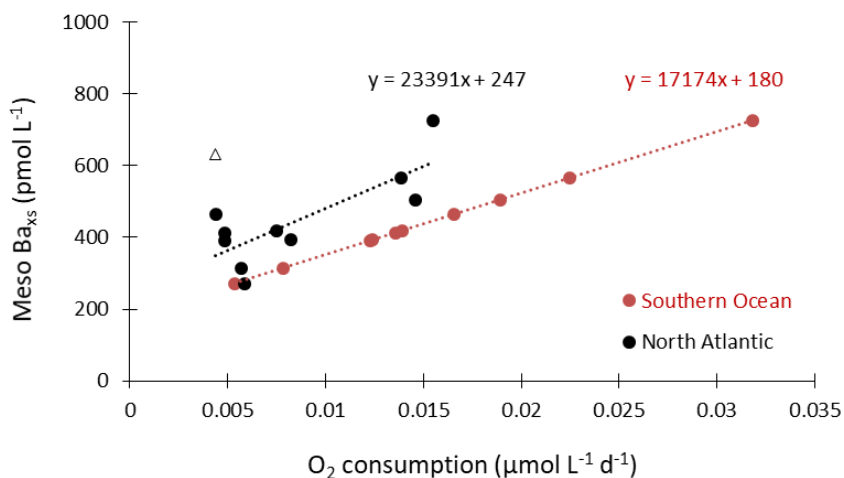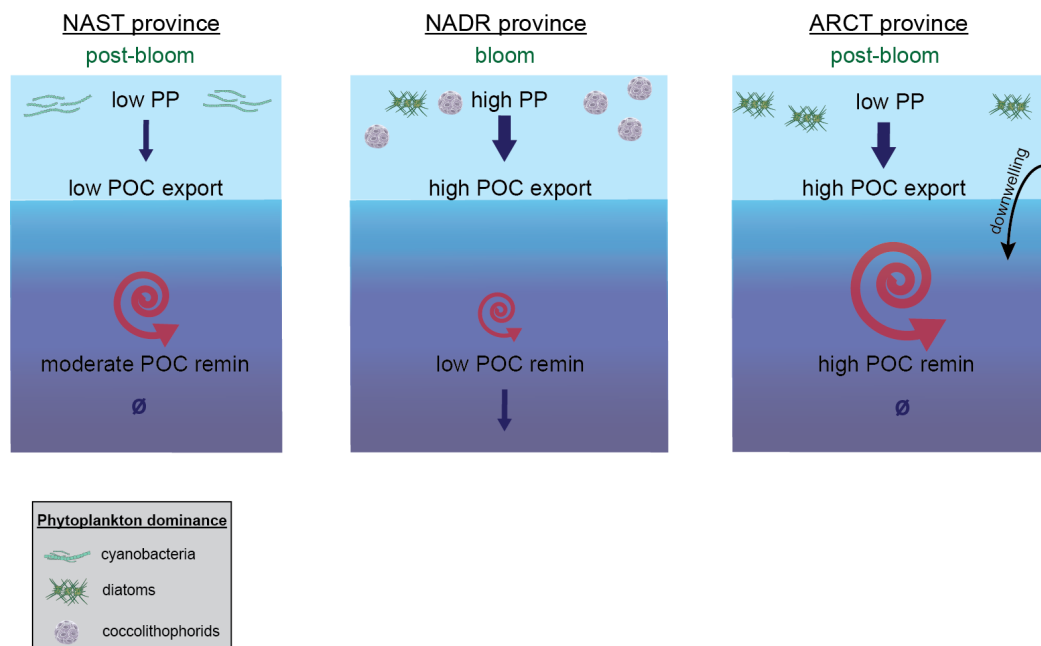
719

720

721

722

723

724

725

726
727

Figure 8: Regression of mesopelagic Ba_{xs} (pmol L^{-1}) versus O_2 consumption rate (µmol L^{-1} d^{-1}) using the Southern Ocean transfer function from Dehairs et al. (1997; red dots) and the transfer function obtained here for the North Atlantic (black dots). Station 44 (triangle) was excluded from the regression.

731

732

733

734

Figure 9: Comparison of POC remineralisation fluxes from this study (circles lined in black) to remineralisation fluxes from literature in the North Atlantic. Note that the cited literature studies used different methods for determining remineralisation fluxes: moored sediment traps (# symbols, Honjo et al., 2008), on-board incubations (° symbols, Giering et al., 2014; Collins et al., 2015); excess barium proxy (* symbols, Brewer et al., unpublished results).

Figure 10: **General schematic of the biological carbon pump during GEOVIDE in the NAST, NADR and ARCT provinces. Primary production (PP) data from A. Roukaerts and D. Fonseca Batista (unpublished data); particulate organic carbon (POC) export fluxes from Lemaitre et al. (in prep.); and POC remineralisation fluxes from this study. The dominating phytoplankton communities and the stage of the bloom are also indicated.**